JBC ACCELERATED COMMUNICATION

Development of a potent high-affinity human therapeutic antibody *via* novel application of recombination signal sequence–based affinity maturation

Received for publication, December 14, 2021 Published, Papers in Press, December 29, 2021,
https://doi.org/10.1016/j.jbc.2021.101533

Agnieszka Kielczewska[1,*], Igor D'Angelo[2], Maria Sheena Amador[1], Tina Wang[1], Athena Sudom[3], Xiaoshan Min[3], Palaniswami Rathanaswami[1], Craig Pigott[4], and Ian N. Foltz[1]

From the [1]Amgen British Columbia, Therapeutic Discovery, Burnaby, British Columbia, Canada; [2]Amgen Inc, Therapeutic Discovery, Thousand Oaks, California, USA; [3]Amgen San Francisco, Therapeutic Discovery, San Francisco, California, USA; [4]Innovative Targeting Solutions, Burnaby, British Columbia, Canada

Edited by Peter Cresswell

Therapeutic antibody development requires discovery of an antibody molecule with desired specificities and drug-like properties. For toxicological studies, a therapeutic antibody must bind the ortholog antigen with a similar affinity to the human target to enable relevant dosing regimens, and antibodies falling short of this affinity design goal may not progress as therapeutic leads. Herein, we report the novel use of mammalian recombination signal sequence (RSS)–directed recombination for complementarity-determining region–targeted protein engineering combined with mammalian display to close the species affinity gap of human interleukin (IL)-13 antibody 731. This fully human antibody has not progressed as a therapeutic in part because of a 400-fold species affinity gap. Using this nonhypothesis-driven affinity maturation method, we generated multiple antibody variants with improved IL-13 affinity, including the highest affinity antibody reported to date (34 fM). Resolution of a cocrystal structure of the optimized antibody with the cynomolgus monkey (or nonhuman primate) IL-13 protein revealed that the RSS-derived mutations introduced multiple successive amino-acid substitutions resulting in a *de novo* formation of a π–π stacking–based protein–protein interaction between the affinity-matured antibody heavy chain and helix C on IL-13, as well as an introduction of an interface-distant residue, which enhanced the light chain–binding affinity to target. These mutations synergized binding of heavy and light chains to the target protein, resulting in a remarkably tight interaction, and providing a proof of concept for a new method of protein engineering, based on synergizing a mammalian display platform with novel RSS-mediated library generation.

Recent advances in experimental and computational methods (1–3) are making it possible to complement well-established *in vivo* and *in vitro* methods of antibody discovery with novel *in silico* approaches to refine affinity and specificity of potential therapeutics (4). The complexities of predicting protein structure and interactions of large molecular weight multichain molecules, however, remain a challenge for the field (5) as is design of improved affinity binding of an antibody to a therapeutically relevant target (6–8). Many currently utilized *in silico* affinity engineering technologies rely on the availability of structures and application of rational design (9, 10), but these approaches are limited for highly complex multipass membrane proteins, where a high-resolution crystal structure may remain elusive, underscoring the need for nonhypothesis-driven affinity maturation approaches.

In humans, antibodies are generated from a heavy-chain (HC) gene and one of two light-chain (LC) genes (kappa or lambda). Sequences encoding antibody variable regions are formed from precursor gene segments in a process called V(D)J recombination. At the HC locus, different combinations of V, D, and J segments (or V and J segments at the LC) are joined together in a manner dependent on recombination signal sequences (RSSs) (11–13), the recombination-activating gene 1 (RAG1)/recombination-activating gene 2 (RAG2) complex (14, 15) and nonhomologous end joining. DNA segments are joined together imperfectly and deletions, insertions, and/or substitutions dependent on terminal deoxynucleotidyl transferase (16, 17) (TdT) and nonhomologous end joining greatly enhance diversity. These mechanisms, in addition to variations in HC–LC pairing, allow B cells to generate large antibody repertoires.

Affinity maturation is a process for improving antibody affinity for a specific antigen. *In vivo*, the immune system enables affinity maturation of antibodies by somatic hypermutation of antibody genes and clonal selection of B cells (18), and V(D)J recombination is restricted to complementarity-determining region 3 (CDR3) diversity generation. *In vitro*, this process can be mimicked by repeated cycles of gene mutation and selection of phage or yeast display libraries (19). RSS is nature's most powerful diversification system that the body leverages for the development of B-cell and T-cell immunological diversity (11). Its adaption to an *in vitro* mammalian protein engineering platform enables mutations resulting in insertions, deletions, and/or substitutions of one or multiple amino acids

* For correspondence: Agnieszka Kielczewska, akielcze@amgen.com.

at any desired position within an antibody or a protein (Fig. S1*A*) and has been applied to *in vitro* T-cell receptor T-cell engineering in the past (20). Here, we apply this mutagenesis strategy to the affinity maturation of a fully human antibody.

Results

Construction of HuTARG mammalian cell surface display libraries for affinity maturation of the anti-IL-13 antibody

HuTARG technology is a novel RSS recombination–based protein engineering platform coupled to cell surface display in a mammalian cell culture system. Briefly, DNA encoding CDRs in the HCs and LCs of antibody 731 (Ab731) were engineered by standard molecular biology methods to contain RSS sites (Figs. 1*A* and S1*A*). The resulting plasmid pool contained individual CDRs, where an RSS integration was targeted; successful integration of RSS signals (21) into each CDR was confirmed by terminal restriction fragment length polymorphism (T-RFLP) (Figs. 1*A* and S1*B*). The resulting constructs were stably integrated as a pool into the HuTARG cell line using the Cre-Lox system (22). HuTARG cells are recombination-competent mammalian cells, where the RAG-1-mediated recombinase activity (14, 23) is induced under tetracycline treatment (24). The induction of recombination results in each cell undergoing a unique rearrangement that involves the removal of the RSS cassette and, in the presence of TdT, double-strand break repair, resulting in imperfect joining of recombined segments followed by sequence variation in human immunoglobulin G (IgG) antibody. This antibody is expressed on the surface of the cells (Fig. 1*B*). As HC and LC sequences were targeted separately, two individual pools of

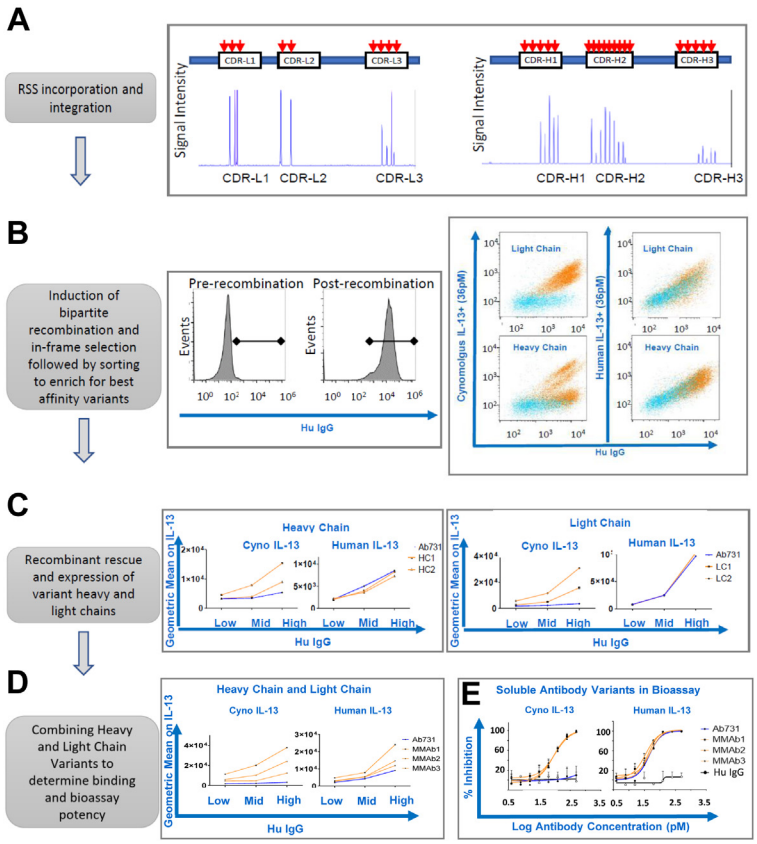

Figure 1. Affinity maturation of a human antibody in the HuTARG platform. *A*, cDNAs encoding heavy chains (HCs) and light chains (LCs) of Ab731 were subjected to standard site-directed mutagenesis methods to engineer recombination signal sequences (RSSs) every second amino-acid position on each CDR (CDR-L1, CDR-L2, CDR-L3, CDR-H1, CDR-H2, and CDR-H3). Successful incorporation of RSS sequences into the CDRs was verified by T-RFLP (see the Supporting methods section). As HC and LC sequences were targeted separately, two individual pools of vectors were generated and integrated into the HuTARG cell line for HC and LC library construction. *B*, for affinity maturation, HuTARG cells undergo bipartite recombination in response to tetracycline induction, which results in "imperfect joining" of diversified segments and expression of in-frame surface immunoglobulin G (IgG). Library complexity is created as each cell potentially expresses a novel rearrangement with unique mutations in IgG. Thus, cell-surface–displayed IgG enables FACS-based enrichments of the libraries for higher affinity than the parental antibody (*left panel*). Three rounds of sorting were done on both HC and LC libraries, resulting in a pool of highly enriched cells that are showing improved binding on NHP IL-13 and have maintained binding to human IL-13 (*right panel*). *C*, recombinantly rescued and cloned HC and LC sequence variants were individually expressed on the surface of HuTARG cells. Transfected cells were stained with 70 pM of NHP or human soluble biotinylated IL-13 protein followed by streptavidin–fluorochrome detection and FACS analysis. Three gates were selected at "IgG+" low, mid, and high gates, which enabled ranking of antibody variants. Parental antibody 731 is shown in *blue*. Best confirmed variants are shown in *orange* for HC (*left panel*) and LC (*right panel*). *D*, HC and LC variants identified in *C* were combined and analyzed for binding to soluble biotinylated IL-13 protein (*left*) or molecularly re-engineered as a soluble secreted antibody, expressed and tested in a bioassay for biological activity (*right*); *E*, normal human dermal fibroblast cells were stimulated by either 250 pM of recombinant human IL-13 or 300 pM of recombinant NHP IL-13 in the presence of titrating amounts of anti-IL-13 antibodies. After 48 h, eotaxin-1 release was determined in culture supernatant and used to determine percent of inhibition for each antibody. cDNA, complementary DNA; CDR, complementarity-determining region; FACS, fluorescence-activated cell sorting; NHP, nonhistone protein; T-RLFP, terminal restriction fragment length polymorphism.

vectors were generated and used to create diversified HC and LC antibody cell surface display libraries. Since recombination occurs in the cell directly and there is no need for a transformation step or individual integration step, the limitation of library complexity is determined by cell number. In this case, we utilized a library complexity of 3.4×10^8 cells for the diversified HC and 3.2×10^6 cells for diversified LC. Improved affinity variants (as determined by higher than parental antibody binding) were isolated by three rounds of fluorescence-activated cell sorting (FACS) by cell-surface staining with 36 pM of recombinant soluble nonhistone protein (NHP) IL-13 (Fig. 1*B*, *right panel*). Variant antibody sequences selected to have improved affinity were found to include insertions and substitutions that were relatively evenly distributed across the enriched LCs consistent with the frequency of RSS integration (Fig. S2).

Relative affinity and potency characterization of diversified anti-IL-13 antibody variants

Rescued antibody sequences were cloned and transiently expressed on the surface of human embryonic kidney 293T (HEK293T) cells to rank their binding to soluble human and NHP IL-13 by FACS analysis (Fig. 1*C*). Geometric mean values of fluorescence for binding to the target protein were compared in three gates based on cell-surface IgG expression (gating strategy is shown in Fig. S3). Of the HC variants that showed improved NHP IL-13 binding, two were confirmed by KinExA (Fig. S4) to have an affinity higher than their parent antibody: HC1 and HC2 (Fig. 1*C* and Table S1). A similar analysis was undertaken for LC variants and resulted in the identification of three LC sequences (LC1, LC2, and LC3) with higher than parental antibody binding (Fig. 1*C* and Table S1). These LC variants were subsequently combined by checkerboard pairing with the best HC variants in all possible permutations (Fig. 1*D*). This resulted in the identification of three antibodies, MMAb1, MMAb2, and MMAb3, which had improved affinity to both NHP and human IL-13 (Fig. 1*D* and Table 1) and showed higher binding than antibodies with individual mutations in the LC or HC. Their biological potency was assessed for neutralization of eotaxin-1 release from normal human dermal fibroblast cells stimulated with human or NHP IL-13. All antibodies were found to be potent inhibitors against both ligands, with EC_{50}s that were limited by the concentration of IL-13 in the assay (Fig. 1*E*). In contrast, the parental Ab731 showed no activity against NHP IL-13.

KinExA-based affinity determination demonstrated that MMAb3 had affinities of 5.1 pM to NHP IL-13 and 34 fM to human IL-13, thus showing a 700-fold improvement and a 56-fold improvement, respectively (Table 1 and Fig. S5).

Crystal structure determination of MMAb3 complexed to NHP IL-13

To understand the molecular determinants of the very high-affinity interaction of the MMAb3 antibody with NHP and human IL-13, we determined the crystal structure of NHP IL-13 in complex with MMAb3 antigen-binding fragment

Table 1
Sequences of highest affinity variants obtained by combining HC and LC mutations aligned with human/cyno IL-13 affinity and potency determination

	LC				HC			Cy IL-13		Hu IL-13	
								K_d (pM)	IC_{50} (pM)	K_d (pM)	IC_{50} (pM)
									95% CI		
Antibody	CDR-L1	CDR-L2	CDR-L3	CDR-H1	CDR-H2	CDR-H3					
Ab731	SGDKLGDKYTC	HDSKRPS	QAWDSSTYV	SYAMS	AFSGSGGSTYYADSVKG	DGLGPYFYNYGMDV		3550 (2310–5340)	>500 (N/A)	1.9 (1.0–3.1)	45.4 (37.9–54.5)
MMAb1 (LC1/HC2)	———————SF	———————	———————	—G—	———————————————	———————————		18.7 (11–32)	93.6 (72.1–121.5)	0.295 (0.09–0.69)	34.7 (27.8–43.3)
MMAb2 (LC2/HC2)	——————————AF	———————	———————	—G—	———————————————	———————————		12.4 (8–19)	102.1 (81.9–127.3)	0.142 (0.03–0.35)	49.0 (40.9–58.8)
MMAb3 (LC1/HC1)	———————SF	———————	———————	———	——WDV————————	———————————		5.1 (3.1–7.9)	90.8 (73.9–111.7)	0.034 (0.002–0.105)	41.3 (35.1–48.7)

Abbreviation: N/A, not applicable.

(Fab) at a resolution of 2.1 Å (Fig. 2*A*, Protein Data Bank [PDB]: 7REW) and subsequently created homology models for MMAb1 and MMAb2 bound to the same ligand. The crystal structure of NHP IL-13 in complex with MMAb3 Fab revealed that the helix-C of IL-13 is oriented parallel to the Fab cleft and is interposed between the Fab HCs and LCs. The total buried solvent-accessible surface area of 1784.8 Å^2 is greater than that observed for average antibody–antigen interfaces (1500–1600 Å^2) (25). The overall shape complementarity score of 0.714 suggests an even higher degree of complementarity for the IL-13–Fab interface than average (0.64–0.68) (26), indicating an extensive and fitted interface for the two molecules. The crystal structure provided an explanation to the high affinity of MMAb3 toward NHP and human IL-13. MMAb3 deviates from the parental Ab731 *via* three consecutive residues in the CDR-H2 (Trp 54/Asp 55/Val 56 *versus* Ser 54/Gly 55/Gly 56) and two successive residues on the CDR-L1 (Ser 32/Phe 33 *versus* Thr 32/Cys 33) (Table 1 and Fig. 2*A*). The first set of residues induces the formation of a π–π stacking channel, wherein the engineered residue Trp 54 from CDR-H2 picks up π–π stacking interactions with Pro 103 of CDR-H2, leading to similar contacts further along the channel with CDR-H2 Tyr 104 and IL-13 residues Pro 72 and His 73 engaging in mostly van der Waals contacts (Fig. 2*C*). It is also likely that the presence of Asp 55 and Val 56 in place of parental Gly 55 and Gly 56 serves to further stabilize the backbone of the CDR-H2 loop, although this was difficult to assess energetically because of the conformational variability associated with the presence of two subsequent Gly residues. The central role of Trp 54 to the binding interface is also evidenced by its buried surface area of 170.1 Å^2, which makes up nearly 10% of the total solvent-accessible surface area. Structural evidence therefore suggests a stabilizing role for Trp 54, rather than being a direct determinant of affinity or specificity; two properties we believe are more likely driven by interactions from the CDR-L1 (Fig. 2*B*). As the MMAb3 and Ab731 CDR-L1 paratopes differ with regard to two residues (Ser 32/Phe 33 *versus* Thr 32/Cys 33), we attempted to identify in this region the change in binding interactions that conferred greater crossreactivity between NHP and human IL-13. In the crystal structure, Asn 68 from NHP IL-13 is positioned between Tyr 31 and the IL-13 backbone carboxyl from residues 73 to 76. The structure suggests that the tight space created by these contacts locks Asn 68 in a conformation that allows binding, albeit through suboptimal hydrogen bonding with Tyr 31 (Fig. 2*D*). In human IL-13, we observed a Ser residue in place of Asn 68 (Fig. 2*E*). Ser 68, given its smaller size and greater distance from the surrounding IL-13 backbone residues, is conformationally less restricted and better positioned to establish a stronger hydrogen bond with the hydroxyl group of Tyr 31, resulting in tighter binding (consistent with experimental data). In either case, and very difficult to predict *a priori*, the conformation of Tyr 31 is likely stabilized by the downstream-engineered residue Phe 33, with the bulky aromatic ring serving the dual purpose of occupying a cavity and preventing rotamer flipping, as opposed to the parental antibody, which has a Cys 33 (Fig. 2, *F* and *G*) and a surrounding cavity. In the context of the parental antibody in complex with human IL-13, the higher affinity of the Ser 68:Tyr 31 interaction favors an outward conformation of Tyr 31 despite the presence of a cavity surrounding Cys 33. This contrasts with NHP IL-13, where the lower affinity of the Asn 68:Tyr 31 interaction allows the tyrosine to swing back and occupy the

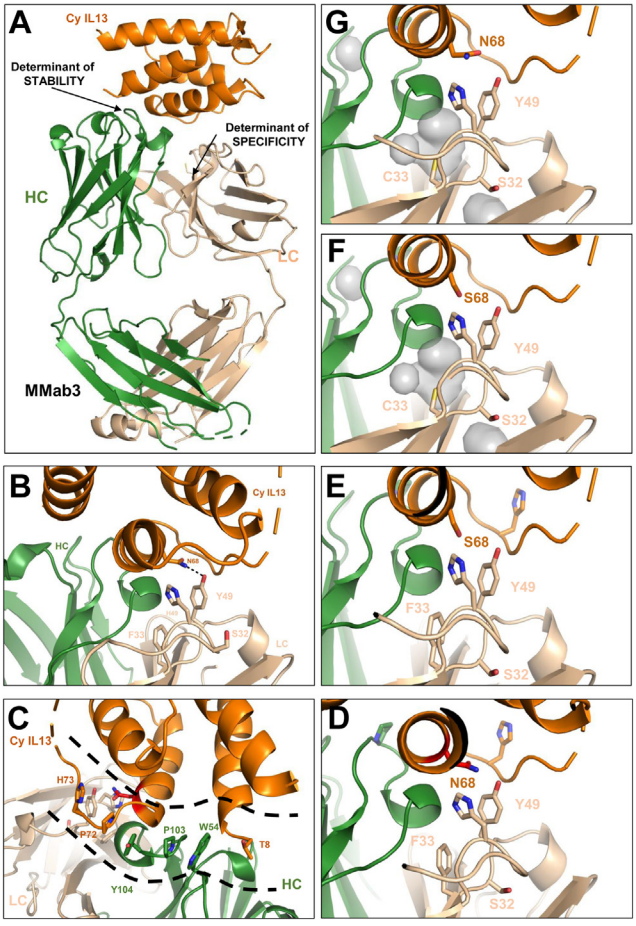

Figure 2. The 2.1 Å cocrystal structure of the NHP IL-13 in complex with the Fab portion of MMAb3 (PDB: 7REW). *A*, the mutated residues implicated in the human/NHP IL-13 crossreactivity are located on the CDR-L1, whereas those providing mostly stabilizing contributions are located on CDR-H2. *B*, overview of the interactions between the light chain (LC) of the MMAb3 and the NHP IL-13, which determine the crossreactive nature of the engineered antibody. The only nonconserved position between human and NHP IL-13 is N68 (S68 in Hu). The movement of Y31 is constrained by the introduction of a bulky residue F33 in the LC variant. Y31 forms a strong hydrogen bond with N68 on IL-13, and in addition, it bridges with the backbone of IL-13. Proximal residue H49 on the LC contributes to this interaction in some crystal forms. *C*, close-up view of the interactions between the heavy chain (and partially LC) of the MMAb3 and the NHP IL-13, which provide greater stabilization of engineered antibody. An array of stacking interactions (mostly VdW driven) is observed. Engineered W54 plays a key role in supporting the formation of this structural feature. *D*, crystal structure of MMAb3 in complex with NHP IL-13. *E*, close-up view of the interactions between the LC of MMAb3 antibody and human IL-13 as predicted based on homology modeling using the determined crystal structure of MMAb3 complexed with NHP IL-13. *F*, model of parental Ab731 in complex with human IL-13. *G*, model of Ab731 in complex with NHP IL-13. In both models of Ab731, C33 is placed in a buried cavity (*gray*), which can be destabilizing and prevent strong binding of Y31 to N68 on NHP IL-13 or S68 on human IL-13. This cavity is filled by the bulkier side chain of F33 in the MMAb3 variant. Ab731, antibody 731; CDR, complementarity-determining region; Fab, antigen-binding fragment; IL-13, interleukin 13; NHP, nonhistone protein; PDB, Protein Data Bank.

cavity surrounding Cys 33, thus reaching an internal energy minimum. This however significantly lowers affinity of the parental antibody toward NHP IL-13. The binding stability of MMAb3 for both human and NHP IL-13 is conferred by several protein–protein interactions not usually identified or detected through standard molecular engineering techniques using computational prediction methods and as confirmed by molecular mechanics–generalized born surface area methods applied to the NHP IL-13 complex structure. Mutations simulated in the region of interest were found to be mostly additive and failed to capture the synergy between the single changes. While we were able to structurally rationalize the benefit of mutations of the LC (Thr 32, Cys 33, to Ser 32, Phe 33) and HC (Ser 54, Gly 55, Gly 56 to Trp 54, Asp 55, Val 56), simulations indicate that an array of other changes could be comparable and are not helpful in formulating a working hypothesis (Supporting information). This is due on one hand to the number and overall length of the stacking interactions (for the stability drivers), and on the other hand, to the intrinsic variability of the CDRs (for the affinity drivers), whose conformation is generally difficult to reliably sample using *in silico* molecular mechanics–based predictive methods or molecular dynamics.

The homology models generated for MMAb1 and MMAb2 are consistent with the structural hypothesis provided previously. MMAb1 and MMAb2 share mutation L-Cys Phe 33, which confers greater affinity toward NHP IL-13 compared with parental Ab731. Neither MMAb1 nor MMAb2 possess a Trp at position 54, which we speculate confers greater stability to the complex. Energetically, these minor changes were captured after the proper insertion was made and the model reminimized (Supporting information).

Discussion

In vitro affinity maturation is a widely used technique to increase affinity of therapeutic protein (antibody) candidates to their targets. Classical technologies employed in the field include targeted (specific residues are mutated) and random (span of Fv fragment is mutated by saturation mutagenesis or error-prone PCR) mutagenesis (27–29). As these methods rely on display technologies dependent on yeast or phage display, the variant library size is limited to a small number of successful bacterial transformations (30). In addition, as the engineering occurs on a molecular level and is subsequently expressed on yeast or bacterial cell, mammalian-specific post-translational modifications or stability determinants will not be recapitulated.

Using an *in vitro* mutagenesis strategy occurring in a mammalian cell, we were able to engineer a fully human therapeutic antibody with the highest affinity reported in the literature without a cocrystal structure to allow a mutagenesis strategy based on rational design. The mutations introduced by RSS-mediated recombination targeting CDRs of the Ab731 resulted in considerable increase in diversity, with the CDR-H3 the least altered, which is perhaps not surprising as CDR-H3 is the principal determinant of epitope recognition for B cells leaving the bone marrow (31). Insertions and deletions were the dominant types of mutations observed in the affinity-enriched FACS sorted cells (Fig. S2).

To our knowledge, the affinity of MMAb3 (as well as MMAb2 at 142 fM) to the human IL-13 protein is one of the highest described in the literature. We previously reported an *in vivo*–generated anti-IL-8 antibody with subpicomolar (610 fM) affinity, measured by KinExA technology (32). Other examples of very high–affinity antibodies include affinity maturation by site-directed mutagenesis of a murine anti-IL-1b antibody, XMA005 and subsequent humanization of that, XOMA 052, yielding subpicomolar antibodies (240 and 300 fM, respectively), measured similarly by KinExA technology (33). An engineered antifluorescein single-chain antibody was also reported to have a K_d of 270 fM to the small-molecule hapten fluorescein, measured similarly by an equilibrium-binding method (34, 35).

Though the structure of IL-13 is known (36), the great benefit of the nonhypothesis-driven RSS mutagenesis–based affinity maturation is that prior structural knowledge was not needed. The RSS-derived mutations are unique and introduced multiple successive amino-acid substitutions, resulting in a *de novo* formation of a π–π stacking–based protein–protein interaction between the affinity-matured HC and the helix C on IL-13, as well as an interface-distant residue Phe 33, which drove the LC-binding affinity to target. These mutations synergistically provide binding contributions from the HCs and LCs, which would have been difficult to engineer *a priori* using *in silico* predictive mutagenesis. Finally, we addressed the NHP toxicology species affinity gap between the therapeutic and surrogate antibody, discovering an affinity-matched molecule to the therapeutic candidate Ab731.

Experimental procedures

Generation of diversified surface library for affinity maturation

Antibody sequence diversification was carried out using RSS recombination in cell culture. Using standard molecular biology techniques, an RSS cassette comprised of a 23 bp RSS, a spacer region of 1.4 kb, and a 12-bp RSS was inserted into a plasmid encoding the HC and LC sequence of the antibody to be affinity matured. This approach was used to construct a set of plasmids, each with an RSS cassette at a unique location within CDR1, CDR2, or CDR3 of the LC. Each RSS cassette contained a Tau restriction site, which was used to confirm successful RSS incorporation into the plasmid by T-RFLP. A similar approach was used to construct a set of plasmids with RSS cassette insertions spanning the HC CDRs. Cre-lox recombination was used to stably integrate single copies of plasmids from each set into the HuTARG mammalian cell line engineered to express TdT and RAG1–RAG2 complex under the control of Tet-inducible promoter.

Induction of RAG-mediated recombination by tetracycline (MilliporeSigma; catalog no.: 58346) resulted in excision of the RSS cassette and the imperfect joining (because of TdT and DNA repair involving nonhomologous end joining) of

antibody sequences leading to variation in length and sequence composition at precise locations within the CDRs. Cells encoding a functional in-frame antibody gene displayed IgG antibody on the cell surface *via* a transmembrane anchor. In-frame joining also resulted in expression of the puromycin resistance marker, which enabled puromycin-based selection cells carrying in-frame antibodies (Enzo Life Sciences; catalog no.: BML-GR312-0050). With this approach, two distinct mammalian display libraries were generated: one with a fixed LC and sequence diversity in the HC CDRs and the other with a fixed HC and sequence diversity in the LC CDRs.

Isolation and characterization of optimized guide antibodies

HC and LC HuTARG recombined libraries were enriched for high-affinity binding to soluble recombinant NHPmolgus IL-13 (Sino Biological, Inc; catalog no.: 11057-CNAH) by multiple rounds of FACS sorts on BD FACS Aria III. The recombined cells along with stable cell line expressing parental Ab731 on the surface were stained with 250 ng/ml of NHP IL-13 followed by detection with antihuman IL-13 mAb IL-13-3-biotin (Mabtech; catalog no.: 3470-6-250) precomplexed with Streptavidin Alexa 647 (Jackson Immunoresearch Labs; catalog no.: 016-600-084). Positive sorting gate was set for a high ratio of NHP IL-13 binding to cell surface antibody expression based on the parental Ab731 stable cell line as a benchmark control to ensure that the population captured represented higher affinity. After three rounds of FACS, the enriched cells were lysed and the antibody sequences were determined by Sanger sequencing. Subsequently, antibodies were cloned as either membrane-tethered cell surface displayed for or standard secreted antibody and expressed in HEK293T cells (American Type Culture Collection).

Ranking of binding of Ab731 affinity-matured variants to NHP IL-13 by FACS

Complementary DNA encoding the antibodies was expressed transiently in HEK293T cells. The cells were cultured at 1×10^6 cells/ml in FreeStyle 293 Expression Medium (Gibco; catalog no.: 12338026) for 3 h on a nontreated tissue cultured in a 6-well plate. Transfection was done using 293fectin Transfection Reagent (Gibco; catalog no.: 12347019) with 1 μg/ml DNA. All samples were analyzed 24 h after transfection along with Ab731 expressed as control. To test for binding to NHP IL-13, cells were stained with 70 pM of recombinant NHPmolgus IL-13 with detection as described previously. To test for binding to human IL-13, cells were stained with 70 pM of biotinylated recombinant human IL-13 protein (R&D Systems, Inc; catalog no.: 213-ILB-100/CF) followed by flow cytometric analysis and geometric mean determination using FlowJo software (Ashland, Oregon-based FlowJo LLC, a subsidiary of Becton Dickinson).

T-RFLP to confirm RSS cassette placement

Pooled vectors encoding RSS cassettes within antibody CDR sequences (HC or LC) were PCR amplified using a 6-carboxyfluorescein-labeled forward primer and an unlabeled reverse primer. Treatment of the resulting amplicon with the restriction enzyme NheI resulted in cleavage at a unique site within the RSS cassette such that the size of the 6-carboxyfluorescein-labeled fragment, determined by fragment analysis (Genewiz USA), determined its location within the antibody sequence: the larger the fragment, the further into the antibody sequence the RSS cassette was placed.

Standard KinExA K_d measurement protocol

KinExA 3200 instrument along with an Autosampler (Sapidyne Instruments) was used to measure the K_d by standard KinExA method (1, 32). Briefly, KinExA experiments for full-affinity characterization were performed by titrating human IL-13 (15 nM–5 fM) or NHP IL-13 (500 nM–250 fM) (32) with a constant concentration of mAb and leaving the reaction to reach equilibrium at room temperature (∼240 C) for 18 to 80 h. The free mAb remaining in the solution at equilibrium was measured by passing the sample over polymethyl methacrylate beads precoated with hIL-13. The bead-captured mAb was detected with goat antihuman IgG (H + L) Alexa 647 as described (32).

For each antibody characterized, a minimum of two experiments were run, using different mAb concentrations to generate an Ab-controlled and a K_d-controlled curve 2. For the femtomolar affinity antibodies, multiple experiments were done taking mAb at 1 nM, 10 pM, 1 pM, 300 fM, and 50 fM concentrations. The experiments were analyzed with the KinExA Pro software in the n-curve analysis module.

Additional experimental procedures are described in the Supporting information section.

Data availability

X-ray crystal structure data that support the finding of this study have been deposited in the Worldwide PDB. The PDB accession code is 7REW. Other data generated for this study are included within this article and supporting information. Any additional information or data are available upon request.

Supporting information—This article contains supporting information (26, 32, 37–45).

Acknowledgments—We thank Irwin Chen and Xin Huang for critical reading on the article and for suggestions. We also thank Shinako Takimoto for technical assistance during this study.

Author contributions—A. K. and I. N. F. conceptualization; C. P. methodology; I. D., S. A., T. W., and P. R. investigation; A. S. and X. M. data curation; A. K., I. D. and I. N. F. writing–original draft.

Conflict of interest—A. K., I. D., S. G., T. W., A. S., X. M., P. R., and I. N. F. are employees and stock holders of Amgen at the time of data collection. C. P. is an employee of Innovative Targeting Solutions. The authors have submitted a patent application based on results covered in the article.

Abbreviations—The abbreviations used are: Ab731, antibody 731; CDR3, complementarity-determining region 3; Fab, antigen-binding fragment; FACS, fluorescence-activated cell sorting; HC, heavy

chain; HEK293T, human embryonic kidney 293T; IgG, immunoglobulin G; IL, interleukin; LC, light chain; NHP, nonhistone protein; PDB, Protein Data Bank; RAG1, recombination-activating gene 1; RAG2, recombination-activating gene 2; RSS, recombination signal sequence; TdT, terminal deoxynucleotidyl transferase; T-RFLP, terminal restriction fragment length polymorphism.

References

1. Baker, D. (2019) What has de novo protein design taught us about protein folding and biophysics? *Protein Sci.* **28**, 678–683
2. Silva, D. A., Yu, S., Ulge, U. Y., Spangler, J. B., Jude, K. M., Labao-Almeida, C., Ali, L. R., Quijano-Rubio, A., Ruterbusch, M., Leung, I., Biary, T., Crowley, S. J., Marcos, E., Walkey, C. D., Weitzner, B. D., *et al.* (2019) De novo design of potent and selective mimics of IL-2 and IL-15. *Nature* **565**, 186–191
3. Koepnick, B., Flatten, J., Husain, T., Ford, A., Silva, D. A., Bick, M. J., Bauer, A., Liu, G., Ishida, Y., Boykov, A., Estep, R. D., Kleinfelter, S., Norgard-Solano, T., Wei, L., Players, F., *et al.* (2019) De novo protein design by citizen scientists. *Nature* **570**, 390–394
4. Nimrod, G., Fischman, S., Austin, M., Herman, A., Keyes, F., Leiderman, O., Hargreaves, D., Strajbl, M., Breed, J., Klompus, S., Minton, K., Spooner, J., Buchanan, A., Vaughan, T. J., and Ofran, Y. (2018) Computational design of epitope-specific functional antibodies. *Cell Rep.* **25**, 2121–2131.e5
5. Vasquez, M., Krauland, E., Walker, L., Wittrup, D., and Gerngross, T. (2019) Connecting the sequence dots: Shedding light on the genesis of antibodies reported to be designed in silico. *mAbs* **11**, 803–808
6. Kiyoshi, M., Caaveiro, J. M., Miura, E., Nagatoishi, S., Nakakido, M., Soga, S., Shirai, H., Kawabata, S., and Tsumoto, K. (2014) Affinity improvement of a therapeutic antibody by structure-based computational design: Generation of electrostatic interactions in the transition state stabilizes the antibody-antigen complex. *PLoS One* **9**, e87099
7. Lippow, S. M., Wittrup, K. D., and Tidor, B. (2007) Computational design of antibody-affinity improvement beyond *in vivo* maturation. *Nat. Biotechnol.* **25**, 1171–1176
8. Mahajan, S. P., Meksiriporn, B., Waraho-Zhmayev, D., Weyant, K. B., Kocer, I., Butler, D. C., Messer, A., Escobedo, F. A., and DeLisa, M. P. (2018) Computational affinity maturation of camelid single-domain intrabodies against the nonamyloid component of alpha-synuclein. *Sci. Rep.* **8**, 17611
9. Kuroda, D., and Tsumoto, K. (2018) Antibody affinity maturation by computational design. *Methods Mol. Biol.* **1827**, 15–34
10. Fischman, S., and Ofran, Y. (2018) Computational design of antibodies. *Curr. Opin. Struct. Biol.* **51**, 156–162
11. Sakano, H., Huppi, K., Heinrich, G., and Tonegawa, S. (1979) Sequences at the somatic recombination sites of immunoglobulin light-chain genes. *Nature* **280**, 288–294
12. Sakano, H., Kurosawa, Y., Weigert, M., and Tonegawa, S. (1981) Identification and nucleotide sequence of a diversity DNA segment (D) of immunoglobulin heavy-chain genes. *Nature* **290**, 562–565
13. Kurosawa, Y., von Boehmer, H., Haas, W., Sakano, H., Trauneker, A., and Tonegawa, S. (1981) Identification of D segments of immunoglobulin heavy-chain genes and their rearrangement in T lymphocytes. *Nature* **290**, 565–570
14. Schatz, D. G., Oettinger, M. A., and Baltimore, D. (1989) The V(D)J recombination activating gene, RAG-1. *Cell* **59**, 1035–1048
15. Oettinger, M. A., Schatz, D. G., Gorka, C., and Baltimore, D. (1990) RAG-1 and RAG-2, adjacent genes that synergistically activate V(D)J recombination. *Science* **248**, 1517–1523
16. Baltimore, D. (1974) Is terminal deoxynucleotidyl transferase a somatic mutagen in lymphocytes? *Nature* **248**, 409–411
17. Desiderio, S. V., Yancopoulos, G. D., Paskind, M., Thomas, E., Boss, M. A., Landau, N., Alt, F. W., and Baltimore, D. (1984) Insertion of N regions into heavy-chain genes is correlated with expression of terminal deoxytransferase in B cells. *Nature* **311**, 752–755
18. Tonegawa, S. (1983) Somatic generation of antibody diversity. *Nature* **302**, 575–581
19. Gai, S. A., and Wittrup, K. D. (2007) Yeast surface display for protein engineering and characterization. *Curr. Opin. Struct. Biol.* **17**, 467–473
20. Oh, J., Warshaviak, D. T., Mkrtichyan, M., Munguia, M. L., Lin, A., Chai, F., Pigott, C., Kang, J., Gallo, M., and Kamb, A. (2019) Single variable domains from the T cell receptor beta chain function as mono- and bifunctional CARs and TCRs. *Sci. Rep.* **9**, 17291
21. Lee, A. I., Fugmann, S. D., Cowell, L. G., Ptaszek, L. M., Kelsoe, G., and Schatz, D. G. (2003) A functional analysis of the spacer of V(D)J recombination signal sequences. *PLoS Biol.* **1**, E1
22. Sauer, B., and Henderson, N. (1988) Site-specific DNA recombination in mammalian cells by the Cre recombinase of bacteriophage P1. *Proc. Natl. Acad. Sci. U. S. A.* **85**, 5166–5170
23. Grawunder, U., Leu, T. M., Schatz, D. G., Werner, A., Rolink, A. G., Melchers, F., and Winkler, T. H. (1995) Down-regulation of RAG1 and RAG2 gene expression in preB cells after functional immunoglobulin heavy chain rearrangement. *Immunity* **3**, 601–608
24. Yao, F., Svensjo, T., Winkler, T., Lu, M., Eriksson, C., and Eriksson, E. (1998) Tetracycline repressor, tetR, rather than the tetR-mammalian cell transcription factor fusion derivatives, regulates inducible gene expression in mammalian cells. *Hum. Gene Ther.* **9**, 1939–1950
25. Chothia, C., and Janin, J. (1975) Principles of protein-protein recognition. *Nature* **256**, 705–708
26. Lawrence, M. C., and Colman, P. M. (1993) Shape complementarity at protein/protein interfaces. *J. Mol. Biol.* **234**, 946–950
27. Tabasinezhad, M., Talebkhan, Y., Wenzel, W., Rahimi, H., Omidinia, E., and Mahboudi, F. (2019) Trends in therapeutic antibody affinity maturation: From in-vitro towards next-generation sequencing approaches. *Immunol. Lett.* **212**, 106–113
28. Fujii, I. (2004) Antibody affinity maturation by random mutagenesis. *Methods Mol. Biol.* **248**, 345–359
29. Lou, J., Geren, I., Garcia-Rodriguez, C., Forsyth, C. M., Wen, W., Knopp, K., Brown, J., Smith, T., Smith, L. A., and Marks, J. D. (2010) Affinity maturation of human botulinum neurotoxin antibodies by light chain shuffling via yeast mating. *Protein Eng. Des. Sel.* **23**, 311–319
30. Winter, G., Griffiths, A. D., Hawkins, R. E., and Hoogenboom, H. R. (1994) Making antibodies by phage display technology. *Annu. Rev. Immunol.* **12**, 433–455
31. Xu, J. L., and Davis, M. M. (2000) Diversity in the CDR3 region of V(H) is sufficient for most antibody specificities. *Immunity* **13**, 37–45
32. Rathanaswami, P., Roalstad, S., Roskos, L., Su, Q. J., Lackie, S., and Babcook, J. (2005) Demonstration of an *in vivo* generated sub-picomolar affinity fully human monoclonal antibody to interleukin-8. *Biochem. Biophys. Res. Commun.* **334**, 1004–1013
33. Owyang, A. M., Issafras, H., Corbin, J., Ahluwalia, K., Larsen, P., Pongo, E., Handa, M., Horwitz, A. H., Roell, M. K., Haak-Frendscho, M., and Masat, L. (2011) XOMA 052, a potent, high-affinity monoclonal antibody for the treatment of IL-1beta-mediated diseases. *mAbs* **3**, 49–60
34. Boder, E. T., Midelfort, K. S., and Wittrup, K. D. (2000) Directed evolution of antibody fragments with monovalent femtomolar antigen-binding affinity. *Proc. Natl. Acad. Sci. U. S. A.* **97**, 10701–10705
35. Midelfort, K. S., Hernandez, H. H., Lippow, S. M., Tidor, B., Drennan, C. L., and Wittrup, K. D. (2004) Substantial energetic improvement with minimal structural perturbation in a high affinity mutant antibody. *J. Mol. Biol.* **343**, 685–701
36. Teplyakov, A., Malia, T. J., Obmolova, G., Jacobs, S. A., O'Neil, K. T., and Gilliland, G. L. (2017) Conformational flexibility of an anti-IL-13 DARPin†. *Protein Eng. Des. Sel.* **30**, 31–37
37. Rathanaswami, P., Richmond, K., Manchulenko, K., and Foltz, I. N. (2011) Kinetic analysis of unpurified native antigens available in very low quantities and concentrations. *Anal. Biochem.* **414**, 7–13
38. Kabsch, W. (2010) Integration, scaling, space-group assignment and post-refinement. *Acta Crystallogr. D Biol. Crystallogr.* **66**, 133–144
39. Winn, M. D., Ballard, C. C., Cowtan, K. D., Dodson, E. J., Emsley, P., Evans, P. R., Keegan, R. M., Krissinel, E. B., Leslie, A. G., McCoy, A., McNicholas, S. J., Murshudov, G. N., Pannu, N. S., Potterton, E. A., Powell, H. R., *et al.* (2011) Overview of the CCP4

suite and current developments. *Acta Crystallogr. D Biol. Crystallogr.* **67**, 235–242
40. McCoy, A. J., Grosse-Kunstleve, R. W., Adams, P. D., Winn, M. D., Storoni, L. C., and Read, R. J. (2007) Phaser crystallographic software. *J. Appl. Crystallogr.* **40**, 658–674
41. Emsley, P., Lohkamp, B., Scott, W. G., and Cowtan, K. (2010) Features and development of Coot. *Acta Crystallogr. D Biol. Crystallogr.* **66**, 486–501
42. Adams, P. D., Afonine, P. V., Bunkoczi, G., Chen, V. B., Davis, I. W., Echols, N., Headd, J. J., Hung, L. W., Kapral, G. J., Grosse-Kunstleve, R. W., McCoy, A. J., Moriarty, N. W., Oeffner, R., Read, R. J., Richardson, D. C., *et al.* (2010) PHENIX: A comprehensive Python-based system for macromolecular structure solution. *Acta Crystallogr. D Biol. Crystallogr.* **66**, 213–221
43. Krissinel, E., and Henrick, K. (2007) Inference of macromolecular assemblies from crystalline state. *J. Mol. Biol.* **372**, 774–797
44. Zhu, K., Day, T., Warshaviak, D., Murrett, C., Friesner, R., and Pearlman, D. (2014) Antibody structure determination using a combination of homology modeling, energy-based refinement, and loop prediction. *Proteins* **82**, 1646–1655
45. Kabsch, W. (2010) XDS. *Acta Crystallogr. D Biol. Crystallogr.* **66**, 125–132